Verification and Validation of Integrated Simulation of Energetic Particles in Toroidal Plasmas

Z. Lin, J. Bao, S. Taimourzadeh, University of California, Irvine, USA (Email: zhihongl@uci.edu)

G. Dong, Princeton Plasma Physics Laboratory, Princeton, USA

Y. Q. Liu, R. C. He, Z. Liu, Fusion Simulation Center, Peking University, Beijing, China

Abstract.

We have developed first-principles capability for global integrated simulation of nonlinear interactions of multiple kinetic-MHD processes by treating both EP and thermal plasmas on the same footing. Verification and validation have been carried out for the gyrokinetic toroidal code (GTC) simulations of EP interactions with thermal plasmas in a DIII-D NBI-heated plasma. GTC kinetic-MHD simulations of EP interactions with thermal plasmas focus on the DIII-D discharge #159243, which is a NBI-heated plasma with many small-amplitude reversed shear Alfven eigenmodes (RSAE) and toroidal Alfven eigenmodes (TAE), significant flattening of the EP profile, and large amplitude microturbulence. Using classical fast ion profile, GTC simulations find that RSAE with n=4 is the dominant instability. The simulated frequencies agree much better with the experimental frequencies at the time of 790ms, rather than 805ms at which time the equilibrium is used in the simulations. The pressure gradients of thermal plasmas make significant contribution to the RSAE growth rates. Using the outward-shifted fast ion profile calculated from a reduced transport model, TAE with n=6 is found to be unstable in the outer edge, consistent with the experimental data. Electron temperature fluctuations and radial phase shifts from simulations show no significant differences with the experimental data for the strong n=4 RSAE, but significant differences for the weak n=6 TAE. Finally, GTC simulations find strong driftwave instability excited by thermal plasma pressure gradients in the core. The most unstable ion temperature gradient (ITG)-like mode is n=20. The linear ITG-like mode amplitude peak at ρ=0.3, but large fluctuations nonlinearly spread to the whole radial domain. These results indicate that RSAE and TAE in this DIII-D experiment could interact nonlinear with each other and with the microturbulence. In the nonlinear simulation of the TAE in DIII-D discharge #142111 near 525ms, the dominant TAE saturation mechanism is the shearing of zonal flow. The effects of zonal current is much smaller than the zonal flow. Zonal fields (zonal flow and zonal current) are nonlinearly forced driven by the TAE three-wave couplings with a growth rate twice the linear TAE growth rate, $\gamma_{ZF}\sim2\gamma_{TAE}$. Localized current sheets with $k_\parallel$=0 but finite n are nonlinearly generated with a growth rate about 3 times of TAE, $\gamma_{NL}\sim3\gamma_{TAE}$. This current sheets is driven by a nonlinear ponderomotive force and can lead to nonlinearly-driven tearing instabilities. The linear TAE mode structures are broken up by the zonal flow nonlinear ExB convection.

I. Introduction

Energetic particle (EP) confinement is a key physics issue for the burning plasma experiment ITER, since ignition relies on self-heating by energetic fusion products (a-particles). EP transport can affect plasma profiles, beam deposition, and current drive, and can erode reactor walls [1]. Due to the strong coupling of EP with burning thermal plasmas, plasma confinement properties in the ignition regime are some of the most uncertain factors when extrapolating from existing tokamaks to the ITER. Fully self-consistent simulation of EP transport and EP coupling with thermal plasmas must incorporate magnetohydrodynamic (MHD) processes with kinetic effects of both EP and thermal plasmas on an equal footing, which requires an integrated kinetic-MHD simulation model based on the gyrokinetic formalism [2]. Coordinated efforts in verification and validation (V&V) are needed to develop the integrated simulation for EP transport due to mesoscale Alfvenic instabilities primarily excited by EP and EP coupling with microturbulences and macroscopic MHD modes mostly driven by thermal plasmas.

Initial V&V studies of the linear gyrokinetic simulations of reversed shear Alfven eigenmodes (RSAE) excited by fast ions from neutral beam injection (NBI) in the advanced tokamak regime of the DIII-D experiment have been carried out [3] by using a gyrokinetic particle code GTC [4], a gyrokinetic continuum code GYRO [5], and a gyro-Landau uid code TAEFL [6]. Good agreements in RSAE frequency, growth rate, and mode structure have been obtained among these initial value simulations, and between simulation results and experimental measurements using electron cyclotron emission imaging (ECEI) [7]. The successful linear V&V lend some degree of confidence to nonlinear gyrokinetic simulations [8-10] that provide new kinetic insights on nonlinear Alfven eigenmode dynamics and EP transport, and help the construction of reduced EP transport models [11-13] which are needed for fast parameter scans, shot-to-shot analysis, and optimization of ITER experiments.

The first-principles simulations and reduced transport models are built upon a hierarchical construction of EP transport prediction based on more fundamental constituents by the progression from linear dispersion relation to nonlinear dynamics and eventually to EP transport. Nonlinear V&V will take on an increased importance as gyrokinetic and kinetic-MHD hybrid simulation models progress from linear to nonlinear simulations for understanding EP confinement properties regarding instability saturation mechanisms, interactions between mesoscale EP turbulence with microturbulence and MHD modes, and EP transport statistics. While it is unlikely that different models will agree in all situations, the regimes of deviation will need to at least be characterized and understood. This is a continuous process since models and computational methods evolve in time. As updated results become available from the first-principles models, they will provide new calibration points for the reduced EP transport models and stimulate their further development.

The V&V studies should use a hierarchical approach, starting with test cases from existing experiments and quantities that are well-diagnosed. For this purpose, an NBI heated low-confinement (L-mode) plasma (DIII-D discharge #159243) with many small amplitude RSAE and TAE (toroidal Alfven eigenmode), significant flattening of the EP profile, and strong microturbulence [14, 15] has been selected as the reference case for V&V studies by the Integrated Simulation of Energetic Particle (ISEP) project, part of the Scientific Discovery through Advanced Computing (SciDAC) initiative. High quality data for the AE structure, frequency, and amplitude as well as the EP distribution, phase-space flows, and intermittent losses are all available from comprehensive DIII-D diagnostics. Taking advantages of these recent experimental progress, the early linear V&V studies [3] have been extended to nonlinear V&V studies of EP transport by using more newly available EP simulation codes and new EP reduced transport models. Linear and nonlinear simulations of AE and microturbulence in this reference case have been carried out by gyrokinetic, kinetic-MHD hybrid, and eigenvalue codes. Modeling of EP transport have also been carried out by reduced transport models. These V&V studies will proceed from linear simulation of instabilities, to nonlinear simulation of saturation mechanisms, to coupling of mesoscale turbulence with microturbulence and MHD modes, and finally to reduced EP transport models. This paper reports the gyrokinetic formulation implemented in GTC for integrated simulation of the energetic particles in burning plasmas, linear V&V studies, and nonlinear physics of TAE saturation by zonal fields.

II. Integrated simulation capability for interactions of multiple kinetic-MHD processes

Energetic particle (EP) pressure gradients in fusion plasmas can readily excite mesoscale EP instabilities such as the Alfven eigenmodes (AEs) and energetic particle modes that drive large EP transport, which can degrade overall plasma confinement and threaten the machine's integrity. EP could strongly influence thermal plasma dynamics including the microturbulence and macroscopic magnetohydrodynamic (MHD) modes. In return, microturbulence and MHD modes can affect EP confinement. We have formulated and verified a conservative scheme solving the exact electron drift kinetic equation for gyrokinetic simulations of kinetic-MHD processes including Alfven eigenmodes, driftwaves, and collisionless tearing modes [16]. Both vector potential and electron perturbed distribution
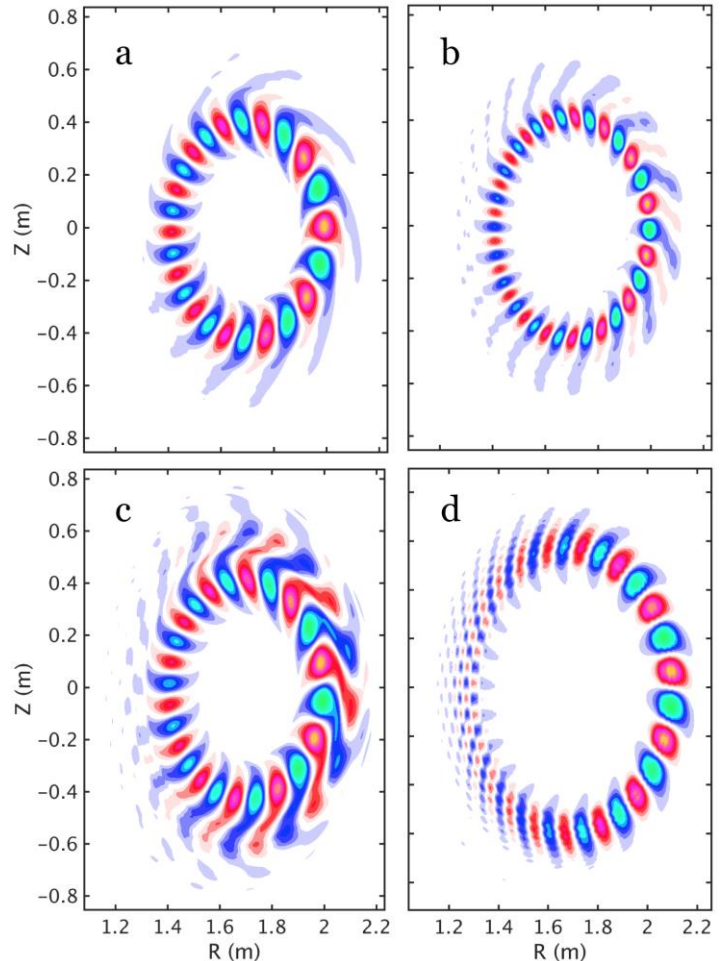
function are decomposed into adiabatic part with analytic solution and non-adiabatic part solved numerically. The adiabatic parallel electric field is solved directly from the electron adiabatic response, resulting in a high degree of accuracy. Since particles are only used to calculate the non-adiabatic response, which is used to calculate the non-adiabatic vector potential through Ohm's law, the conservative scheme minimizes the electron particle noise and mitigates the cancellation problem. Linear dispersion relations of the kinetic Alfven wave and the collisionless tearing mode in cylindrical geometry have been verified in GTC simulations, which show that the perpendicular grid size can be larger than the electron collisionless skin depth when the mode wavelength is longer than the electron skin depth.

The compressional component of magnetic perturbation $\delta B_{//}$ can play an important role in drift-Alfvenic instabilities in tokamaks, especially as the plasma β increases (β is the ratio of kinetic pressure to magnetic pressure). We have formulated and verified a gyrokinetic particle simulation model [17] incorporating $\delta B_{//}$. GTC simulations of drift-Alfvenic instabilities shows that the kinetic ballooning mode (KBM) growth rate decreases more than 20% when $\delta B_{//}$ is neglected for β_e=0.02, and that $\delta B_{//}$ has stabilizing effects on the ion temperature gradient instability, but negligible effects on the collisionless trapped electron mode. The KBM growth rate decreases about 15% when equilibrium current is neglected.

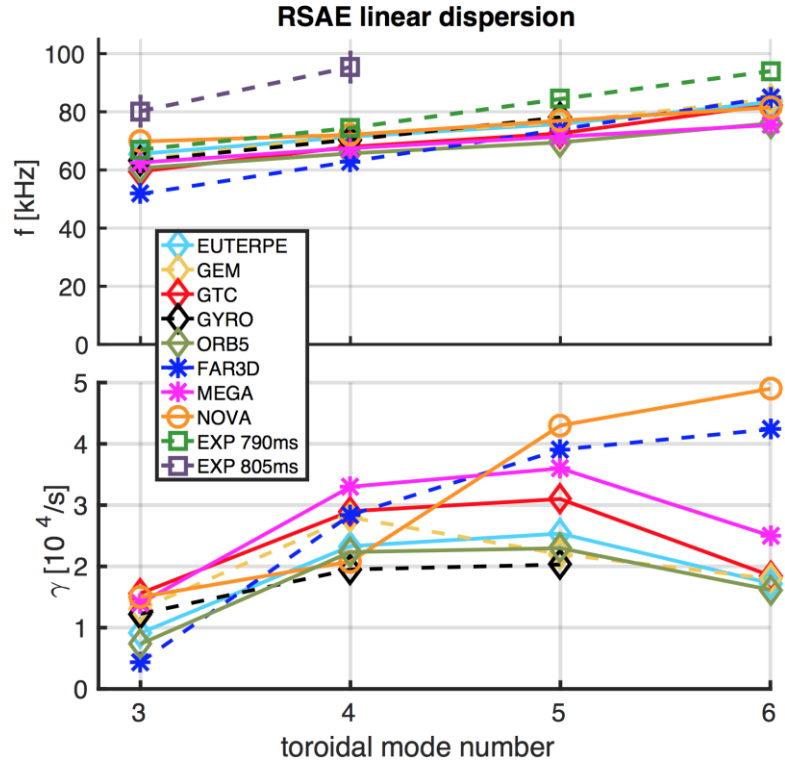## III.   Linear verification and validation of EP interactions with thermal plasmas

EP interactions with thermal plasmas can lead to the excitations of various AEs ranging from low frequency beta-induced Alfven-acoustic eigenmode (BAAE) and beta-induced Alfven eigenmode (BAE), to high frequency RSAE and TAE. All these AEs have been successfully verified in global GTC simulations. In particular GTC simulations find that realistic EP density gradients can simultaneously excite BAAE and BAE, with similar radial mode widths and comparable linear growth rates even though damping rate of BAAE is much larger than BAE in the absence of EPs [18]. These AEs can interact nonlinearly with each other, and with microtutubulence driven by thermal plasmas. Therefore, integrated simulation of multiple kinetic-MHD processes by treating both EP and thermal plasmas on the same footing need to be verified and validated.

Fig. 1. Perturbed electrostatic potential from GTC simulations of DIII-D shot 159243.00805. (a-b) n = 4 and n = 6 simulations, respectively, using a fast ion density profile calculated from kinetic EFIT. (c-d) n = 4 and n = 6 simulations, respectively, using a fast ion density profile calculated from the kick model.

We present GTC linear simulations of RSAE and TAE observed in DIII-D shot #159243. Since fast ion profiles have the biggest uncertainty among all equilibrium profiles measured in the experiment, we use the fast ion profiles both from the kinetic EFIT reconstruction [19] accounting only collisional transport, and from the more realistic the kick model [13] taking into account EP transport by RSAE and TAE. These two EP profiles are used in GTC simulations of n = 4 and n = 6 modes, which are the most prominent RSAE and TAE modes, respectively, observed in the experiment. Fig. 1 shows the simulated 2D modes structures of the perturbed electrostatic potential for these four simulations. The top row shows the n = 4 and 6 mode structures, both of which show an unstable RSAE, with no TAE, obtained using the kinetic EFIT profile. The bottom row shows a transition of the dominant mode from RSAE to TAE as the toroidal mode number increases from n = 4 to n = 6. The dominant n = 4 RSAE with a radial domain of ρ= 0.3 - 0.6 (square-root of normalized toroidal flux function) is accompanied by a lower amplitude TAE with a radial domain of ρ=0.6 - 0.9, consistent with the ECE data.

Fig. 2. Linear dispersion relation calculation for RSAE in DIII-D shot 158243 at 805 ms. (a) Real frequencies. (b) Growth rates. The plot markers are diamond, star, and circle for the gyrokinetic, kinetic-MHD hybrid, and perturbative eigenvalue codes, respectively. (Figure reproduced from Ref.20)
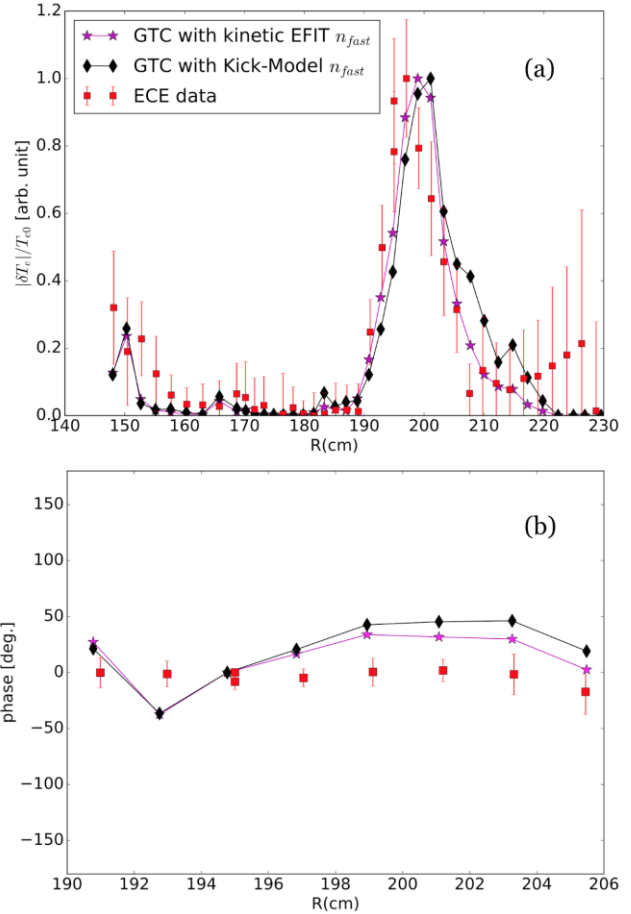
In a linear V&V [20], GTC linear simulation results are compared with initial value gyrokinetic codes (EUTERPE [21], GEM [22], GYRO, ORB5 [23]), two initial value kinetic-MHD codes (FAR3D [24], MEGA [25]), and a perturbative eigenvalue code (NOVA-K [26]). Using the EFIT fast ion profile, all simulation codes find that RSAE is the dominant instability. The real frequencies from all eight codes shown in Fig. 2 have a coefficient of variation (CV) less than 5% for the most unstable modes with toroidal mode number n = 4 and 5. The simulated frequencies agree much better with the ECE frequencies at the experimental time of 790ms, rather than the 805ms at which time the equilibrium is used in the simulations. This is probably due to limitations in the accuracy of the safety factor q_{min} calculated in the EFIT reconstruction. The simulated growth rates of these two RSAE exhibit greater variations with a CV up to 17% for the five gyrokinetic codes, and a CV up to 26% for all eight codes. Mode structures of the dominant modes agree well among all seven non-perturbative codes regarding radial eigenmodes, 2D shape on poloidal plane, ballooning characteristics, radial extent, and radial symmetry breaking. Using the outward-shifted fast ion profile from the kick model, all codes find the n = 6 TAE to be the dominant instability in the outer edge, consistent with the ECE data. Variations of the real frequencies and growth rates from seven simulation codes are slightly larger than those of the RSAE, partially due to the co-existence of multiple radial eigenmodes with similar frequencies and growth rates.

GTC simulation data have been processed by the Synthetic Diagnostic Platform (SDP) [27] to produce electron temperature fluctuations and radial phase shifts, which show no significant differences

for the strong n = 4 RSAE, but significant differences for the weak n = 6 TAE. Fig. 3(a) shows |dTe/Te0|, of the n=4 mode obtained from GTC via SDP, for both the kinetic EFIT (black) and kick model (magenta) fast-ion density profiles and the experimental data (red). All three structures show peak amplitude near R=198cm. The full width half max are nearly the same, with that from the kick-model being slightly larger. These results show there is no significant difference in RSAE mode structures between simulations and the experimental data. The experimental data may indicate the presence of radially increasing fluctuations between R = [210, 220] cm, which may correspond to TAE activity; however, the uncertainty in the data is large in that region. Fig. 3(b) shows the mode's phase difference for different radial locations, relative to R = 195.0cm, for the experimental data and the GTC simulations with the kinetic EFIT and kick model fast ion density profiles. The disagreement between the phase values for the GTC simulations in the outer radial regions is due to the presence of a subdominant TAE near R=215cm in the simulation using the kick model fast ion density.

Fig. 3. Comparison of GTC simulation data, after being processed through the Synthetic-Diagnostic-Platform, to experimental ECE data for DIII-D #159243 at 805 ms. (a) Radial structure of |dTe/Te0|. (b) The phase profile relative to R = 195.0 cm. (Figure reproduced from Ref.20)

Finally, GTC simulations find strong driftwave instability excited by thermal plasma pressure gradients in the core. The most unstable ion temperature gradient (ITG)-like mode is $n=20$ and has $\omega_r=118$KHz and $\gamma=4.5\times10^4$s^{-1}. The linear ITG-like mode amplitude peak at $\rho=0.3$, but large fluctuations nonlinearly spread to the whole radial domain. These results indicate that RSAE and TAE in this DIII-D experiment could interact nonlinear with each other and with the microturbulence. GTC simulations treating both microturbulence and RSAE/TAE on the same footing will be compared with high quality DIII-D data for the eigenmode structure, frequency, and amplitude as well as the EP distribution, phase-space flows, and intermittent EP losses. These linear provide a necessary foundation for the next step of nonlinear V&V studies.

IV.   Nonlinear simulations of TAE saturation via zonal fields

In this section, we extend our previous linear simulation [28] of the n=3 TAE in DIII-D discharge #142111 near 525ms to the nonlinear regime to study the nonlinear saturation of TAE. We have performed simulations to test separately the effects of EP nonlinearity, thermal plasma nonlinearity, and zonal fields. When only EP nonlinearly is kept in the simulation, TAE saturates at high amplitude due to the relaxation of EP density profiles. When thermal plasma nonlinearity is added in the simulation, TAE saturates at lower amplitude, indicating the importance of the thermal plasma nonlinearity. Finally, when zonal fields (zonal flow and zonal current) are self-consistently kept in the simulation, TAE saturates at

much lower amplitude with a much lower EP transport level (Fig. 4), and there is little relaxation in EP density profiles. The effects of zonal fields are mostly by the zonal flow, i.e., suppressing zonal current causes little difference in the TAE saturation amplitude.

The nonlinear simulation results including the zonal fields are summarized in Fig.4 for the zonal components of both $\delta\phi$ and $\delta A_{\parallel}$. In the early linear phase, the zonal fields are dominated by the numerical noise from non-zonal components, as proven by the convergence tests on the number of particles per cell in the simulation. Thus the zonal fields grow approximately with the same growth rates as the linear instability of the non-zonal components. Once the TAE amplitude exceeds a certain threshold, the zonal fields grow exponentially with twice the linear TAE growth rate, $\gamma_{ZF}\sim2\gamma_{TAE}$, regardless of the numerical parameter we choose. These results indicate that the zonal fields are nonlinearly forced driven by the TAE three-wave couplings, rather than generated through the nonlinear modulational instability, in which case the growth rate of the zonal fields should be proportional to the amplitude of the pump wave (non-zonal components). The zonal field generation is thus passive, similar to earlier MHD-gyrokinetic simulations [29, 30]. The collisionless skin depth effects likely suppress the modulational instability. The growth rate of the zonal fields is slightly less than twice of the TAE growth rate, indicating some damping of the zonal fields by background plasmas. The amplitude of zonal magnetic field associated with the zonal current is much smaller than zonal electric field associated with the zonal flow. These results demonstrate that the dominant TAE saturation mechanism is by the shearing of the zonal flow.
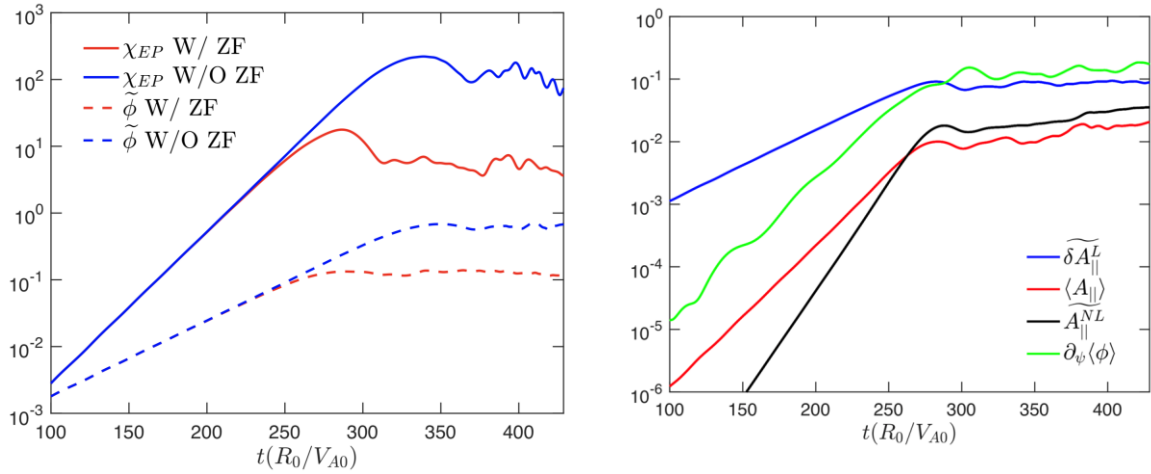

Fig.4 Time history for EP heat conductivity χ_{EP} and TAE electrostatic potential ϕ in simulations with or with self-consistently generated zonal fields (left panel), and (right panel) electrostatic potential of zonal flow $<\phi>$, vector potentials for zonal current $<A_{\parallel}>$, TAE $A_{\parallel}$, and localized current $A_{\parallel}^{NL}$.

Fig. 4 also shows that vector potential associated with current sheets $A_{\parallel}^{NL}$ with n=3 and $k_{\parallel}$=0 localized to rational surfaces are nonlinearly generated with a growth rate about 3 times of TAE, $\gamma_{NL}\sim3\gamma_{TAE}$. This current sheet with $k_{\parallel}$=0 but finite n is driven by a nonlinear ponderomotive force (dynamo effects in MHD terminology) in the non-adiabatic part of the electron momentum equation (or generalized Ohm's law) [16], which also drive the zonal current with n=m=0. This localized current sheet can lead to nonlinearly-driven tearing instabilities as recently observed in MHD-gyrokinetic hybrid simulations [31].

The TAE mode structures are shown in Fig. 5. The linear eigenmode has a typical ballooning structure (left panel). The up-down symmetry of the ideal MHD mode structure is broken by the nonperturbative EP contribution, which introduces the radial symmetry breaking due to the radial variations of EP density gradients [6, 23]. However, after nonlinear saturation, the mode structures are broken up by the zonal flow with radially localized structures (middle panel). Even when zonal fields are

removed in the simulation, the TAE mode structures are eventually broken up by nonlinear ExB convection (right panel).
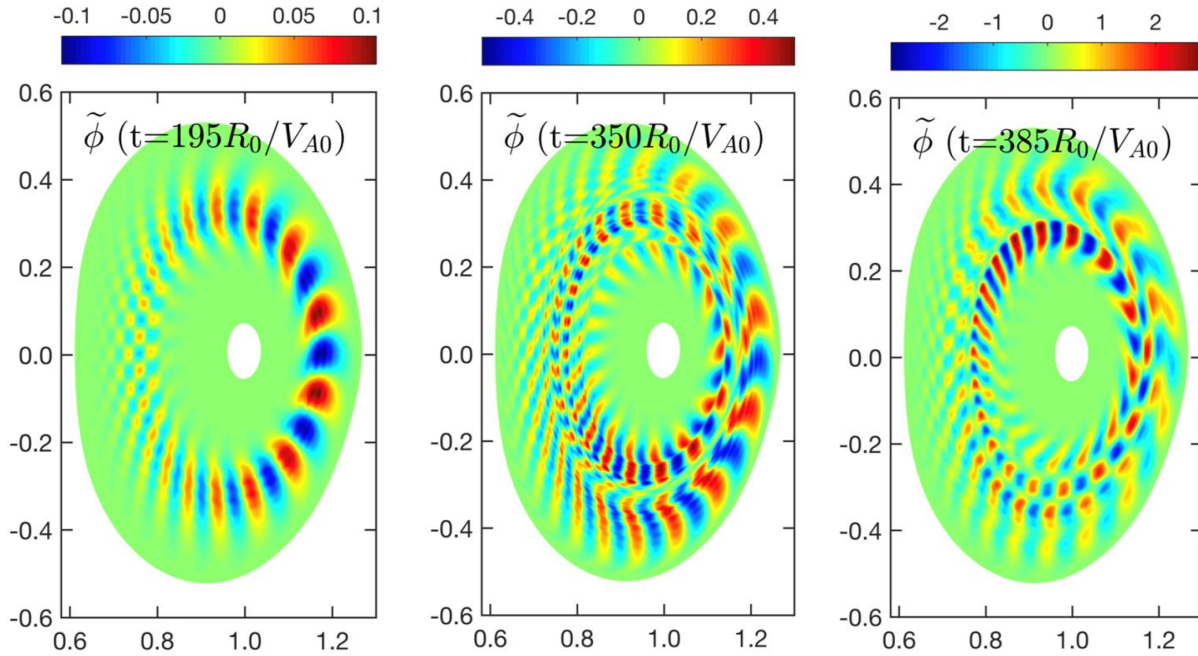

Fig.5. *Poloidal contour plots of n=3 TAE electrostatic potential φ in linear phase (left panel), nonlinear phase in simulation with zonal fields (middle panel), and nonlinear phase in simulation without zonal fields. The indicated time on each penal corresponds to the time in the left panel of Fig. 4 for the evolution of φ.*

References:

[1] D. C. Pace, W. W. Heidbrink, and M. A. Van Zeeland, Physics Today 68, 10 (2015).
[2] L. Chen and F. Zonca, Reviews of Modern Physics 88, 015008 (2016).
[3] D. A. Spong et al, Physics of Plasmas19, 082511 (2012).
[4] Z. Lin et al, Science, vol. 281, 1835 (1998).
[5] J. Candy and R. Waltz, Journal of Computational Physics 186, 545 (2003).
[6] D. Spong, B. Carreras, and C. Hedrick, Physics of Fluids B: Plasma Physics 4, 3316 (1992).
[7] M. A. Van Zeeland et al, Phys. Rev. Letters 97, 135001 (2006).
[8] E. Bass and R. Waltz, Physics of Plasmas 17, 112319 (2010).
[9] H. Zhang et al., Physical review letters 109, 025001 (2012).
[10] Y. Chen et al, Physics of Plasmas 20, 012109 (2013).
[11] E. M. Bass and R.Waltz, Physics of Plasmas 24, 122302 (2017).
[12] N. N. Gorelenkov et al, Nuclear Fusion 58, 082016 (2018).
[13] M. Podesta et al, Plasma Physics and Controlled Fusion 59, 095008 (2017).
[14] C. Collins et al, Physical review letters 116, 095001 (2016).
[15] W. Heidbrink et al, Phys. Plasmas, vol. 24, p. 056 109, 2017.
[16] J. Bao, D. Liu, Z. Lin, *Phys. Plasmas* **24**, 102516 (2017).

[17] Ge Dong *et al*, *Phys. Plasmas* **24**, 081205 (2017).

[18] Yaqi Liu, Zhihong Lin, Huasen Zhang, Wenlu Zhang, *Nuclear Fusion* **57**, 114001 (2017).

[19] L. Lao et al, Nuclear Fusion 30, 1035 (1990).

[20] *Verification and validation of integrated simulation of energetic particles in fusion plasmas I: linear simulations*, S. Taimourzadeh, E. M. Bass, Y. Chen, C. Collins, N. N. Gorelenkov, A. Konies, Z. X. Lu, D. A. Spong, Y. Todo, M. E. Austin, J. Bao, A. Biancalani, M. Borchardt, A. Bottino, W. W. Heidbrink, Z. Lin, R. Kleiber, A. Mishchenko, L. Shi, J. Varela, R. E. Waltz, G. Yu, W. L. Zhang, and Y. Zhu, in preparation (2018).

[21] A. Mishchenko et al, Physics of Plasmas 21, 092110 (2014).

[22] Y. Chen and S. E. Parker, Journal of Computational Physics 189, 463 (2003).

[23] S. Jolliet et al, Computer Physics Communications 177, 409 (2007).

[24] J. Varela, D. Spong, and L. Garcia, Nuclear Fusion 57, 046018 (2017).

[25] Y. Todo and T. Sato, Physics of Plasmas 5, 1321 (1998).

[26] C. Z. Cheng and M. S. Chance, Phys. Fluids 29, 3695 (1986).

[27] L. Shi et al, Review of Scientific Instruments 87, 11D303 (2016).

[28] Zhixuan Wang et al., Phys. Rev. Lett. 111, 145003 (2013).

[29] Y. Todo, H.L. Berk B.N. Breizman, Nuclear Fusion 50, 084016 (2010).

[30] Spong D.A., Carreras B.A. and Hedrick C.L., Phys. Plasmas 1, 1503 (1994).

[31] Nature Communications 9, 3282 (2018).